Available online at www.sciencedirect.com

ScienceDirect

IFAC PapersOnline CONFERENCE PAPER ARCHIVE

IFAC PapersOnLine 51-12 (2018) 6–11

A Predictive Guidance Algorithm for Autonomous Asteroid Soft Landing ⋆

Julio C. Sanchez* **Francisco Gavilan*** **Rafael Vazquez***

* *Departamento de Ingenieria Aeroespacial, Universidad de Sevilla, 41092, Seville, Spain (e-mails: jsanchezm@us.es, fgavilan@us.es, rvazquez1@us.es).*

Abstract: The objective of this work is to present a closed-loop guidance algorithm for landing a probe on an irregular shaped rotating asteroid. The main assumption is that the spacecraft is orbiting close to the asteroid and has a continuous propulsion system enabling it to do a powered descent. The goal is to minimize fuel consumption while avoiding collision with the asteroid during the manoeuvre. This non-convex time-continuous optimal control problem is transformed to a convex static program by relaxing some constraints, discretizing and using an iterative method to handle with the asteroid gravity field non-linearities. Then, a guidance algorithm based on Model Predictive Control is applied with the purpose of coping with unmodelled dynamics and disturbances. Numerical results are showed and discussed.

Keywords: Spacecraft autonomy, Trajectory planning, Optimal trajectory, Constrained control.

1. INTRODUCTION

Soft landing on small bodies is one of the benchmark problems of the guidance, navigation and control discipline. Recent examples include NEAR, Hayabusa and Rosetta missions, see Dunham et al. (2002); Kubota et al. (2006); Canalias et al. (2014). Nowadays, NASA's OSIRIS REX mission is on-going and will collect and return samples of Bennu asteroid, see NASA (2016).

However, missions with the purpose of landing on small body objects face several challenges from a control point of view. The irregular shape, density or rotation of these bodies induce severe non-linearities in the equations of motions, see Werner and Scheeres (1996) or Scheeres et al. (1998). Moreover, the model parameters are not exactly known until the orbiter reaches the asteroid or comet. This is the reason why many missions spend long times orbiting the body with the purpose of characterizing it. Additionally, the distance from Earth creates a time delay which makes impossible ground control during the descent phase. Therefore, autonomous on-board algorithms are required to cope with uncertain parameters and possible disturbances. This consideration makes Model Predictive Control (MPC) techniques suitable to be employed when designing guidance methods for descent trajectories.

Looking at past landing missions, different techniques (from a propulsive point of view) have been employed. NEAR landed on Eros with four pre-planned open-loop braking impulses, see Dunham et al. (2002). Hayabusa landed on Itokawa with a powered descent trajectory based on state feedback, see Kubota et al. (2006). However, Philae achieved touchdown with Churyumov-Gerasimenko following a pure ballistic trajectory, see Canalias et al. (2014). On the other hand, powered descent trajectories shall be considered for landers with limited-thrust capabilities.

MPC schemes require fast trajectory computation. Lossless convexification techniques, which have been applied for designing Mars landing in Acikmese and Ploen (2007), rendezvous operations in Lu and Liu (2013) and asteroid landing in Pinson and Lu (2015), seem promising to be applied for close-loop guidance. These techniques combine a relaxation approach to convexify non-convex constraints and an iterative method to tackle the non-linearities of the gravity field by solving a second-order cone programming problem (SOCP) at each iteration.

The main contribution of this paper is an algorithm that optimizes fuel consumption while providing a safe landing trajectory in the presence of disturbances. Additionally, a two-phase descent trajectory is considered by splitting the manoeuvre in a circumnavigation phase followed by a landing phase as in Dunham et al. (2016), thus increasing flexibility when choosing the departure point.

The structure of this paper is as follows. Section 2 describes the asteroid model. Next, Section 3 presents the landing problem with its constraints and the objective function. Section 4 describes the techniques used to solve the optimal control problem. Section 5 describes the designed MPC scheme which allow close-loop guidance. Section 6 shows results for cases of interest. Finally, Section 7 closes this paper with some additional considerations.

2. ASTEROID MODELLING

Consider a spacecraft in the vicinity of an asteroid, the relative position $\mathbf{r}=[x,y,z]^T$ and mass m of the lander in an asteroid fixed frame coincident with its principal inertia axes (where z has the largest moment of inertia and x the

⋆ The authors gratefully acknowledge Universidad de Sevilla for funding part of this work through its V-PPI US. Rafael Vazquez acknowledges financial support of the Spanish Ministerio de Economía y Competitividad under grant MTM2015-65608-P.

10.1016/j.ifacol.2018.07.080

lowest) and whose origin is the asteroid center of mass, are governed by

$$\ddot{\mathbf{r}} = -\dot{\boldsymbol{\omega}} \times \mathbf{r} - 2\boldsymbol{\omega} \times \dot{\mathbf{r}} - \boldsymbol{\omega} \times (\boldsymbol{\omega} \times \mathbf{r}) + (\mathbf{F} + \mathbf{T})/m, \quad (1)$$

$$\dot{m} = -\|\mathbf{T}\|_2 / v_{ex}, \quad (2)$$

where $\boldsymbol{\omega}$ is the asteroid rotation rate, $\mathbf{F}$ the external forces acting on the lander, $\mathbf{T}$ the thrust control action and v_{ex} the associated escape gases velocity. The most relevant force term in the vicinity of a small body is its central gravity field which can be modelled with several approaches, in terms of potential. Asteroid gravity force can be easily computed from gravitational potential as $\mathbf{F}_g = m\nabla U_g$.

2.1 Polyhedron model

The exterior gravitational potential of a constant-density polyhedron was derived analytically by Werner and Scheeres (1996),

$$U_g = \frac{G\rho}{2} \left(\sum_{e \in edges} \mathbf{r}_e^T \mathbf{E}_e \mathbf{r}_e L_e - \sum_{f \in faces} \mathbf{r}_f^T \mathbf{F}_f \mathbf{r}_f w_f \right), \quad (3)$$

where G is the universal gravitation constant, ρ is the asteroid bulk density, $\mathbf{r}_e$ is a vector from the field point to an arbitrary point on each edge, $\mathbf{E}_e$ is a dyad defined in terms of the face and edge normal vectors associated to each edge, L_e is a logarithmic term expressing the potential of a 1D straight line, $\mathbf{r}_f$ is a vector from the field point to an arbitrary point on each face, $\mathbf{F}_f$ is the outer product of face normal vectors and w_f is the solid angle subtended by a face when viewed from the field point. The main advantage of this model is its capability of giving the exact exterior potential of the polyhedron anywhere. However, its main drawback is the computational effort required to cover all edges and faces of the polyhedron.

2.2 Mass-concentrations model

The gravitational potential of n point masses is

$$U_g = \sum_{i=1}^{n} \frac{G m_i}{\|\mathbf{r} - \mathbf{r}_i\|_2}, \quad (4)$$

where m_i is the point mass value and $\mathbf{r}_i$ the point mass position. This model provides a good enough accuracy when the number of point masses is adequate and are placed within the limits of the small body. Additionally, its main advantages are the possibility of modelling non-uniform density bodies and the lower computational effort when compared with the polyhedron model. This model was used for Hayabusa mission, see Kubota et al. (2006).

The mass-concentrations model is used for the optimal control computation whereas the most accurate polyhedron potential is used in simulations to consider gravity model uncertainties (although the asteroid shape is assumed to be known). The well-known spherical harmonic expansion is not considered for landing operations because it might diverge close to the asteroid surface.

3. LANDING PROBLEM FORMULATION

This section introduces the objective function and constraints.

3.1 Constraints of the problem

Thruster constraints

Once the engine is turned on, it is assumed to be throttleable between a maximum and a minimum magnitude (T_{max} and $T_{min}>0$) as it cannot be turned off for safety until the descent is completed, see Pinson and Lu (2015)

$$T_{min} \leq \|\mathbf{T}\|_2 \leq T_{max}. \quad (5)$$

Note that the lower bound of this constraint is non-convex.

Surface avoidance constraint

Avoiding collision with the asteroid when descending is a non-convex constraint also. However, this constraint can be convexified considering two consecutive phases (circumnavigation and landing) as in Dunham et al. (2016).

Circumnavigation phase

When the spacecraft is far from the landing point, $\mathbf{r}_F$ which is known, it must circumnavigate the asteroid without colliding with it. This non-convex constraint can be convexified by using a rotating tangent plane to the asteroid surface. Since the asteroid has an irregular shape, the minimum volume ellipsoid circumscribing the object is considered to be avoided

$$(\mathbf{r}(t) - \mathbf{r}_t(t))^T \mathbf{n}_t(t) \geq \mathbf{0}, \quad t \in [t_0, t_0 + t_{circ}], \quad (6)$$

where $\mathbf{r}_t$ is a point on the ellipsoid surface, $\mathbf{n}_t$ is the normal vector to the ellipsoid at $\mathbf{r}_t$ and t_{circ} is the circumnavigation phase duration.

The tangent plane rotation must be imposed beforehand. A spherical linear interpolation to move the plane between the departure point, $\mathbf{r}_0$, and the landing point, $\mathbf{r}_F$, has been considered, see Fig.1 for a 2D example.

Landing phase

Once the spacecraft has finished the circumnavigation phase and is near the landing point, a line of sight area (LOS) composed by five planes emanating from the landing point is considered for sensing purposes. In local axes centered at the landing point, this region is defined as $y' \geq c_x(x' - x'_0)$, $y' \geq -c_x(x' + x'_0)$, $y' \geq c_z(z' - z'_0)$, $y' \geq -c_z(z' + z'_0)$ and $y' \geq 0$, where y' is assumed to be the approach axis. This is expressed as

$$\mathbf{A}_L(\mathbf{r}(t) - \mathbf{r}_F) \leq \mathbf{b}_L, \quad t \in [t_0 + t_{circ}, t_f], \quad (7)$$

where $\mathbf{A}_L \in \mathbb{R}^{5\times3}$ and $\mathbf{b}_L \in \mathbb{R}^5$ summarize the equations of the LOS region planes algebraically.

Fuel consumption constraint

The probe has a limited amount of fuel to spend. At any time the spacecraft mass is greater than its dry mass

$$m(t) \geq m_{dry}. \quad (8)$$

Terminal constraints

The spacecraft has to reach the desired landing point $\mathbf{r}_F$ with null relative velocity at the specified final time, t_f

$$\mathbf{r}(t_f) = \mathbf{r}_F, \quad \mathbf{v}(t_f) = \mathbf{0}. \quad (9)$$

3.2 Objective function

The chosen objective function, J, minimizes fuel consumption or equivalently maximizes the final mass value

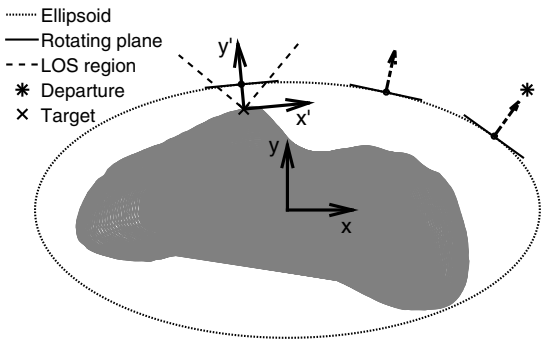

Fig. 1. Surface avoidance constraint.

$$J = -m(t_f). \tag{10}$$

4. OPTIMAL CONTROL COMPUTATION

In this section, the solution method to the optimal control problem governed by (1)-(2), the constraints given by (5)-(9) and the objective function defined in (10) is presented. The asteroid is assumed to be rotating uniformly around its major inertia axis, z. However, the presented formulation can be extended to time-varying rotating bodies.

4.1 Change of variables

Following Acikmese and Ploen (2007), a variable change is used to deal with the non-convex thrust constraint

$$\mathbf{a}_t = \mathbf{T}/m, \quad a_{tm} = \|\mathbf{T}\|_2/m, \tag{11}$$

and the mass variable is also changed to

$$q = \ln(m). \tag{12}$$

which combined with (11) leads to a linear fuel consumption equation, $\dot{q}{=}{-}a_{tm}/v_{ex}$. Equations (11)-(12) relax the non-convex constraint (5) as

$$T_{min}e^{-q} \leq a_{tm} \leq T_{max}e^{-q}, \tag{13}$$

$$\|\mathbf{a}_t\|_2 \leq a_{tm}, \tag{14}$$

where (13) can be posed as a linear constraint if the mass term is linearized around a reference value, q_r, as; $e^{-q}{\approx}e^{-q_r}(1{-}(q{-}q_r))$. Equation (14) constitutes a second-order cone constraint which is convex. It can be shown that relaxation does not alter the original problem (details can be found in Acikmese and Ploen (2007)). Using the new variables, the time-continuous optimization problem is

$$\begin{aligned}
\min_{\mathbf{a}_t, a_{tm}} \quad & -q(t_f), \\
\text{s.t.} \quad & \dot{\mathbf{r}}(t) = \mathbf{v}, \\
& \dot{\mathbf{v}}(t) = -2\boldsymbol{\omega} \times \mathbf{v} - \boldsymbol{\omega} \times (\boldsymbol{\omega} \times \mathbf{r}) + \mathbf{a}_t \\
& \qquad +\nabla U_g(\mathbf{r}), \\
& \dot{q}(t) = -a_{tm}/v_{ex}, \\
& q(t) \geq q_{dry}, \\
& a_{tm}(t) \geq T_{min}e^{-q_r(t)}[1-(q(t)-q_r(t))], \\
& a_{tm}(t) \leq T_{max}e^{-q_r(t)}[1-(q(t)-q_r(t))], \\
& \|\mathbf{a}_t(t)\|_2 \leq a_{tm}(t), \\
& \mathbf{r}_t^T(t)\mathbf{n}_t(t) \leq \mathbf{r}^T(t)\mathbf{n}_t(t), \quad t \in [t_0, t_0+t_{circ}], \\
& \mathbf{A}_L\mathbf{r}(t) \leq \mathbf{b}_L - \mathbf{A}_L\mathbf{r}_F, \ t \in (t_0+t_{circ}, t_f], \\
& \mathbf{r}(t_f) = \mathbf{r}_F, \\
& \mathbf{v}(t_f) = \mathbf{0},
\end{aligned}$$

where time dependencies at the right-hand side of the dynamics equations have been omitted for clarity.

4.2 Problem discretization

The most challenging aspect of the optimization problem are the non-linearities induced by the asteroid gravitation force. This issue is solved using an iterative method where the gravity gradient is evaluated with data from previous computations. The states equations can be rearranged as

$$\dot{\mathbf{x}}^{[j]} = \mathbf{A}\mathbf{x}^{[j]} + \mathbf{B}\mathbf{u}^{[j]} + \mathbf{c}(\mathbf{r}^{[j-1]}), \tag{15}$$

where j is an iteration counter (which will be omitted from now on for clarity, non-linear terms are supposed to be known beforehand), $\mathbf{x}{=}[\mathbf{r}^T, \mathbf{v}^T, q]^T$ represents the full state, $\mathbf{u}{=}[\mathbf{a}_t^T, a_{tm}]^T$ groups the control terms, the matrices $\mathbf{A}$ and $\mathbf{B}$ are expressed as

$$\mathbf{A} = \begin{bmatrix} 0 & 0 & 0 & 1 & 0 & 0 & 0 \\ 0 & 0 & 0 & 0 & 1 & 0 & 0 \\ 0 & 0 & 0 & 0 & 0 & 1 & 0 \\ \omega^2 & 0 & 0 & 0 & 2\omega & 0 & 0 \\ 0 & \omega^2 & 0 & -2\omega & 0 & 0 & 0 \\ 0 & 0 & 0 & 0 & 0 & 0 & 0 \\ 0 & 0 & 0 & 0 & 0 & 0 & 0 \end{bmatrix}, \ \mathbf{B} = \begin{bmatrix} 0 & 0 & 0 & 0 \\ 0 & 0 & 0 & 0 \\ 0 & 0 & 0 & 0 \\ 1 & 0 & 0 & 0 \\ 0 & 1 & 0 & 0 \\ 0 & 0 & 1 & 0 \\ 0 & 0 & 0 & -v_{ex}^{-1} \end{bmatrix},$$

and the vector of non-linear terms $\mathbf{c}$ is given by

$$\mathbf{c} = -\sum_{i=1}^{n} \frac{Gm_i}{\|\mathbf{r}-\mathbf{r}_i\|_2^3} \begin{bmatrix} 0 \\ 0 \\ 0 \\ (x-x_i) \\ (y-y_i) \\ (z-z_i) \\ 0 \end{bmatrix}. \tag{16}$$

Discretizing the manoeuvre time into N intervals of duration $\Delta T{=}(t_f{-}t_0)/N$, a trapezoidal rule can be used to integrate the states equations between nodes

$$\begin{aligned}
\mathbf{x}_k = \ & \mathbf{x}_{k-1} + \Delta T[\mathbf{A}(\mathbf{x}_k + \mathbf{x}_{k-1}) \\
& +\mathbf{B}(\mathbf{u}_k + \mathbf{u}_{k-1}) + \mathbf{c}_k + \mathbf{c}_{k-1}]/2,
\end{aligned} \tag{17}$$

and solving for $\mathbf{x}_k$

$$\begin{aligned}
\mathbf{x}_k = \ & (\mathbf{I} - \Delta T\mathbf{A}/2)^{-1}[(\mathbf{I} + \Delta T\mathbf{A}/2)\mathbf{x}_{k-1} \\
& +(\mathbf{B}(\mathbf{u}_k + \mathbf{u}_{k-1}) + \mathbf{c}_k + \mathbf{c}_{k-1})\Delta T/2],
\end{aligned} \tag{18}$$

where $\mathbf{I}$ is the identity matrix. Defining the following constant matrices

$$\mathbf{C} = (\mathbf{I} - \Delta T\mathbf{A}/2)^{-1}(\mathbf{I} + \Delta T\mathbf{A}/2), \tag{19}$$

$$\mathbf{D} = (\mathbf{I} - \Delta T\mathbf{A}/2)^{-1}\Delta T\mathbf{B}/2, \tag{20}$$

$$\mathbf{E} = (\mathbf{I} - \Delta T\mathbf{A}/2)^{-1}\Delta T/2, \tag{21}$$

a more clear expression of $\mathbf{x}_k$ is found

$$\mathbf{x}_k = \mathbf{C}\mathbf{x}_{k-1} + \mathbf{D}(\mathbf{u}_k + \mathbf{u}_{k-1}) + \mathbf{E}(\mathbf{c}_k + \mathbf{c}_{k-1}). \tag{22}$$

4.3 Compact formulation

For simplicity, following Vazquez et al. (2017), a compact formulation is employed using (22) recursively. Defining the following stack vectors $\mathbf{x_S}{\in}\mathbb{R}^{7N}$ and $\mathbf{u_S}{\in}\mathbb{R}^{4(N+1)}$ as

$$\mathbf{x_S} = \left[\mathbf{x}_1^T, \ldots, \mathbf{x}_N^T\right]^T, \ \mathbf{u_S} = \left[\mathbf{u}_0^T, \ldots, \mathbf{u}_N^T\right]^T, \tag{23}$$

and the following stack matrices

$$\mathbf{F}=\begin{bmatrix}\mathbf{C}\\ \mathbf{C}^2\\ \vdots\\ \mathbf{C}^N\end{bmatrix},\ \mathbf{H}=\begin{bmatrix}\mathbf{E}(\mathbf{c}_1+\mathbf{c}_0)\\ \mathbf{E}(\mathbf{c}_2+\mathbf{c}_1)+\mathbf{C}\mathbf{E}(\mathbf{c}_1+\mathbf{c}_0)\\ \vdots\\ \sum_{j=1}^{N}\mathbf{C}^{N-j}\mathbf{E}(\mathbf{c}_j+\mathbf{c}_{j-1})\end{bmatrix}, \quad (24)$$

$$\mathbf{G}=\begin{bmatrix}\mathbf{D} & \mathbf{D} & \mathbf{\Theta}_{7\times4} & \dots & \mathbf{\Theta}_{7\times4}\\ \mathbf{C}\mathbf{D} & (\mathbf{I}+\mathbf{C})\mathbf{D} & \mathbf{D} & \dots & \mathbf{\Theta}_{7\times4}\\ \vdots & \vdots & \vdots & \ddots & \vdots\\ \mathbf{C}^{N-1}\mathbf{D} & \mathbf{C}^{N-2}(\mathbf{I}+\mathbf{C})\mathbf{D} & \mathbf{C}^{N-3}(\mathbf{I}+\mathbf{C})\mathbf{D} & \dots & \mathbf{D}\end{bmatrix}$$

where $\mathbf{\Theta}$ is a matrix full of zeros. The states propagation equation is posed in a compact form as

$$\mathbf{x_S}=\mathbf{F}\mathbf{x}_0+\mathbf{G}\mathbf{u_S}+\mathbf{H}. \quad (25)$$

The optimization problem compactly expressed is

$$\begin{aligned}\min_{\mathbf{u_S}}\ & -q_N,\\ \text{s.t. }\ & \mathbf{A}_{Tmin}\mathbf{u_S}\ \geq\ \mathbf{b}_{Tmin},\\ & \mathbf{A}_{Tmax}\mathbf{u_S}\ \leq\ \mathbf{b}_{Tmax},\\ & \|\mathbf{a}_{t,k}\|_2\ \leq\ a_{tm,k},\quad k=1\dots N,\\ & \mathbf{A}_{CS}\mathbf{x_S}\ \leq\ \mathbf{b}_{CS},\\ & \mathbf{A}_{LS}\mathbf{x_S}\ \leq\ \mathbf{b}_{LS},\\ & \mathbf{A}_{M}\mathbf{x_S}\ \leq\ \mathbf{b}_{M},\\ & \mathbf{r}_N\ =\ \mathbf{r}_F,\\ & \mathbf{v}_N\ =\ \mathbf{0},\end{aligned} \quad (26)$$

where $\mathbf{A}_{Tmin}$, $\mathbf{A}_{Tmax}\in\mathbb{R}^{N+1\times4(N+1)}$ and $\mathbf{b}_{Tmin}$, $\mathbf{b}_{Tmax}\in\mathbb{R}^{N+1}$ stack the lower and upper thrust bounds respectively, see (13). The matrix $\mathbf{A}_{CS}\in\mathbb{R}^{N_C\times7N}$ and vector $\mathbf{b}_{CS}\in\mathbb{R}^{N_C}$, where N_C is the number of intervals for which the constraint is active, stack the circumnavigation constraint (6), whereas the matrix $\mathbf{A}_{LS}\in\mathbb{R}^{5(N-N_C)\times7N}$ and vector $\mathbf{b}_{LS}\in\mathbb{R}^{5(N-N_C)}$ stack the landing phase constraint (7). Finally, the matrix $\mathbf{A}_M\in\mathbb{R}^{N\times7N}$ and vector $\mathbf{b}_M\in\mathbb{R}^N$ stack the fuel consumption constraint (8). Note that there is a one-to-one relation between $\mathbf{x_S}$ and $\mathbf{u_S}$ given by (25), hence the compact formulation reduces the problem size from $11N+4$ to $4(N+1)$ decision variables. The optimization problem (26) constitutes a SOCP which is equivalent to a convex quadratically constrained linear program.

4.4 Optimal control computation

A states propagation linearized model is used to propagate the trajectory, thus an iterative process where the non-linear asteroid force term is evaluated with the previous computed trajectory, until a desired convergence is reached, has to be developed:

Step 1: Evaluate the asteroid gravity force at all nodes with the initial spacecraft position, $\mathbf{r}_0$. Consider the vehicle flying at minimum thrust to have an initial mass reference, $m_{r,k}=m_0-k\Delta T(T_{min}/v_{ex})$.
Step 2: Compute a solution of the SOCP problem (26).
Step 3: Update the iterations counter j by one. Go to Step 2, using $\mathbf{r}_k^{[j-1]}$ and $m_k^{[j-1]}$, until $\max(\mathbf{r}_k^{[j-1]}-\mathbf{r}_k^{[j-2]})$ <Tol or $j>j_{max}$.

5. MPC GUIDANCE

Autonomous landing guidance requires a closed-loop method to cope with model uncertainties and disturbances. A MPC scheme with a receding horizon (to ease the computational load when approaching landing) is proposed. The terminal constraints (9) are relaxed considering them in the objective function, as quadratic costs, to avoid infeasibility issues when the planning horizon decreases

$$J_{MPC}=-q_N+\gamma_r(\mathbf{r}_N-\mathbf{r}_F)^T\mathbf{I}(\mathbf{r}_N-\mathbf{r}_F)+\gamma_v\mathbf{v}_N^T\mathbf{I}\mathbf{v}_N, \quad (27)$$

where γ_r and γ_v are positive scalars measuring the relative weight between fuel consumption, landing accuracy and touchdown velocity respectively. The MPC algorithm is

Step 1: Obtain the solution of the SOCP problem (26) applying the algorithm of section 4.4.
Step 2: Apply the commanded thrust for the current interval k. Decrease the planning horizon, N, by one.
Step 3: The disturbances will perturb the planned path, so the trajectory is recomputed with the objective function (27) and without terminal constraints. Go to Step 2 until the planning horizon ends..

The previous interval planned trajectory and mass are employed to evaluate the asteroid gravity and the thruster constraints when using the algorithm of section 4.4 to recompute. This reduces the number of required iterations.

6. SIMULATION RESULTS

6.1 Simulation parameters

It is important to remark that although a translational linear model, derived from the mass-concentrations model (4), has been used for the optimal control computation, the simulations showed in this section have been performed with the non-linear polyhedral gravity model (3).

The chosen asteroid is 433 Eros since its shape and parameters, ρ=2.67 g/cm^3 and T_{rot}=5.27 h, are well known from the NEAR mission, see Gaskell (2008) and Yeomans et al. (2000). The mass-concentrations gravity model uses a grid of n=4841 equidistant point-masses within the limits of the asteroid. The point-masses values are taken all equal to $m_i=\rho V/n$, where V is the asteroid volume computed from its polyhedron shape model.

The lander characteristics are chosen to be similar to the NEAR Shoemaker probe, m_0=600 kg with m_{dry}=487 kg, whereas its hydrazine thrusters provide T_{max}=80 N and T_{min}=20 N with v_{ex}=2000 m/s. LOS parameters are chosen as $x_0'=z_0'$=10 m and $c_x=c_z=1/\tan(\pi/4)$. The landing point is chosen to be one of the vertex of Eros shape model, $\mathbf{r}_F=[-0.5114,-2.836,1.443]^T$ km whereas initial position and velocity assume a "circular" equatorial orbit around Eros, $\mathbf{r}_0=[0,35,0]^T$ km and $\mathbf{v}_0=[-3.5709,0,0]^T$ m/s. The manoeuvre time is taken as t_f=2000 s with N=100 sampling intervals which results in discretized periods of ΔT=20 s. The circumnavigation phase is chosen to have a duration of 1500 s, which implies N_C=75, hence the landing phase will last the final 500 s.

6.2 Disturbances modelling

Following Gavilan et al. (2012), disturbances on each thruster component are added to test the MPC scheme of Section 5. This disturbance is modelled as

$$\mathbf{T}=\mathbf{\Omega}(\boldsymbol{\delta\theta})[\bar{\mathbf{T}}(1+\boldsymbol{\delta})+\boldsymbol{\delta}\mathbf{T}], \quad (28)$$

where $\bar{\mathbf{T}}$ is the commanded output computed by the control laws, $\mathbf{\Omega}$ is a rotation matrix, $\boldsymbol{\delta\theta}\sim N_3(\bar{\boldsymbol{\delta\theta}}, \mathbf{\Sigma}_{\delta\theta})$ is a vector of random small angles, $\boldsymbol{\delta}\sim N_3(\bar{\boldsymbol{\delta}}, \mathbf{\Sigma}_{\delta})$ is a vector of multiplicative noises to the computed thrust and $\boldsymbol{\delta}\mathbf{T}\sim N_3(\bar{\boldsymbol{\delta}}\mathbf{T}, \mathbf{\Sigma}_{\delta T})$ is a vector of additive noises. These disturbances model several physical aspects. First, the attitude control of the chaser will not be perfect, so one can expect some alignment errors, modeled by $\mathbf{\Omega}(\boldsymbol{\delta\theta})$ in a simplified way. On the other hand, with $\boldsymbol{\delta}$ and $\boldsymbol{\delta}\mathbf{T}$ one can model thrust level disturbances or even unmodelled forces such as solar gravity force or solar radiation pressure.

The disturbance means are $\bar{\boldsymbol{\delta\theta}}=\mathbf{0}$, $\bar{\boldsymbol{\delta}}=[0.01,\ 0.01,\ 0.01]^T$ and $\bar{\boldsymbol{\delta}}\mathbf{T}=[0.01,\ 0.01,\ 0.01]^T T_{max}$, and the covariances are $\mathbf{\Sigma}_{\delta\theta,ij}=0.0436\delta_{ij}$, $\mathbf{\Sigma}_{\delta,ij}=0.05\delta_{ij}$ and $\mathbf{\Sigma}_{\delta T,ij}=0.02T_{max}\delta_{ij}$.

6.3 Results

Simulations have been done in MATLAB with *Gurobi* optimization package as a second-order cone programming solver. To ease the computational burden of the polyhedron model, asteroid gravity force computation has been coded in C as in Lantoine and Braun (2006). The MPC cost function parameters are chosen as $\gamma_r=\gamma_v=100$ whereas the maximum number of iterations and stop tolerance are taken as $j_{max}=6$ and $\text{Tol}=0.02\|\mathbf{r}_F\|_2$ respectively.

As shown in Fig.2, Fig.3 and Fig.4, collision with the asteroid is avoided and a soft landing on Eros is achieved. The distance to the desired landing point is 8.4378 m and touchdown velocity is 0.9356 m/s which is a good enough result for soft landing (NEAR landed at 1.5-1.8 m/s, see Dunham et al. (2002)) considering the applied disturbances on the thrust components, see Fig.6.

The thrust-norm profile is of the type bang-bang with the switches happening at the start and end of each phase (circumnavigation and landing). As a consequence, the mass evolution maintains a linear decreasing profile with five different zones that match with maximum and minimum thrust-norm values, see Fig.5.

7. CONCLUSIONS

A MPC guidance algorithm to autonomously land powered probes on small bodies while handling with unmodelled dynamics and disturbances has been presented. Lossless convexification, discretization and a successive solution method were employed to solve the asteroid landing control problem. Future work may include comparisons with other state of the art methods, a detailed sensitivity analysis with model parameters as well as including the circumnavigation and landing times as decision variables. Additionally a six-degrees of freedom lander model with attitude control (e.g. reaction wheels or a RCS) shall be considered. This would provide an adequate orientation of the spacecraft landing gear at the touchdown.

ACKNOWLEDGEMENTS

The authors acknowledge Manuel Sanjurjo Rivo, David Morante and Pablo Machuca from Univ. Carlos III de Madrid (Spain) for the gravity model MATLAB scripts.

REFERENCES

Acikmese, B. and Ploen, S. (2007). Convex programming approach to powered descent guidance for mars landing. *Journal of Guidance, Control and Dynamics*, 30(5), 1353–1366.

Canalias, E., Blazquez, A., Jurado, E., and Martin, T. (2014). Philae descent trajectory computation and landing site selection on comet churyumov-gerasimenko. In *Proceedings of International Symposium on Spaceflight Dynamics*. Laurel, Maryland, United States of America.

Dunham, D.W., Farquhar, R.W., V.McAdams, J., Holdrige, M., Nelson, R., Whittenburg, K., Antreasian, P., Chesley, S., Helfrich, C., Owen, W.M., Williams, B., Veverka, J., and Harch, A. (2002). Implementation of the first asteroid landing. *Icarus*, 159(2), 433–438.

Dunham, W., Petersen, C., and Kolmanovsky, I. (2016). Constrained control for soft landing on an asteroid with gravity model uncertainty. In *American Control Conference*. Boston, Maryland, United States of America.

Gaskell, R.W. (2008). Gaskell eros shape model v.1.0. In *NASA Planetary Data System*.

Gavilan, F., Vazquez, R., and Camacho, E.F. (2012). Chance-constrained model predictive control for spacecraft rendezvous with disturbance estimation. *Control Engineering Practice*, 60, 111–122.

Kubota, T., Hashimoto, T., Tamura, M., Bando, N., Uo, M., Shirakawa, K., Morita, H., Kominato, T., and Kagawuchi, J. (2006). Flight results on gnc in final descent phase for hayabusa touchdown. In *ISAS 16th Workshop on Astrodynamics and Flight Mechanics*. Japan.

Lantoine, G. and Braun, R.D. (2006). Optimal trajectories for soft landing on asteroids. In *AE8900 MS Special Problems Report*. Space Systems Design Lab, Georgia Institute of Technology.

Lu, P. and Liu, X. (2013). Autonomous trajectory planning for rendezvous proximity operations by conic optimization. *Journal of Guidance, Control and Dynamics*, 36(2).

NASA (2016). OSIRIX-REx mission. `https://solarsystem.nasa.gov/missions/osirisrex`.

Pinson, R. and Lu, P. (2015). Rapid generation of optimal asteroid powered descent trajectories via convex optimization. In *AAS/AIAA Astrodynamics Specialist Conference*.

Scheeres, D., Ostro, S., Hudson, R., DeJong, E., and S.Suzuki (1998). Dynamics of orbits close to asteroid 4179 toutatis. *Icarus*, 132(1), 53–79.

Vazquez, R., Gavilan, F., and Camacho, E.F. (2017). Pulse-width predictive control for ltv systems with application to spacecraft rendezvous. *Control Engineering Practice*, 20, 199–210.

Werner, R.A. and Scheeres, D.J. (1996). Exterior gravitation of a polyhedron derived and compared with harmonic and mascon gravitation representations of asteroid 4769 castalia. *Celestial Mechanics and Dynamical Astronomy*, 65(3), 313–344.

Yeomans, D.K., Antreasian, P.G., Barriot, J.P., Chesley, S.R., Dunham, D.W., Farquhar, R.W., Giorgini, J.D., Helfrich, C.E., Konopliv, A.S., McAdams, J.V., Miller, J.K., Owen, W.M., Scheeres, D.J., Thomas, P.C., Veverka, J., and Williams, B.G. (2000). Radio science results during the near-shoemaker spacecraft rendezvous with eros. *Science*, 289(5487), 2085–2088.

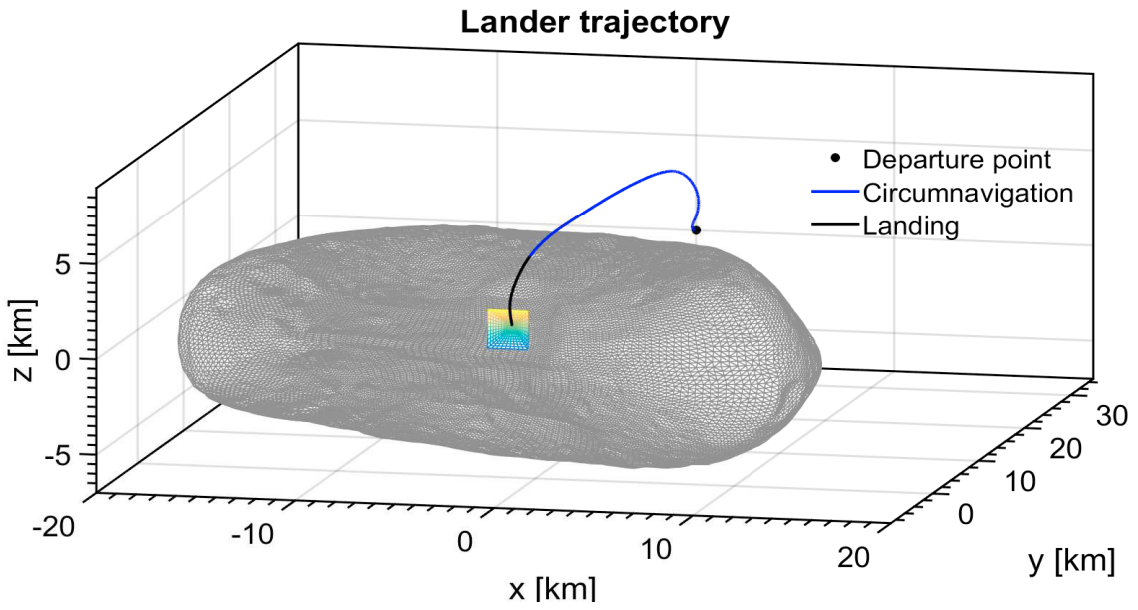

Fig. 2. Lander path on the asteroid frame.

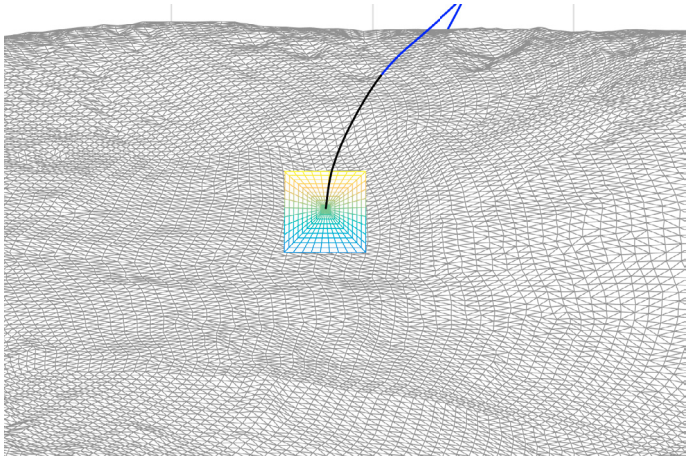

Fig. 3. Landing trajectory detail.

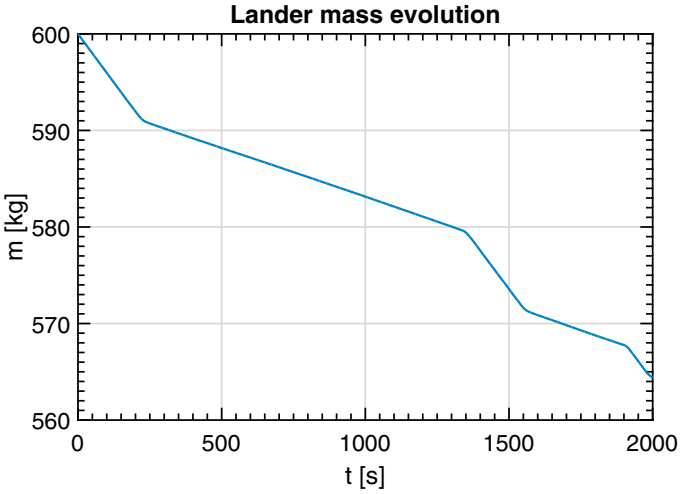

Fig. 5. Lander mass evolution.

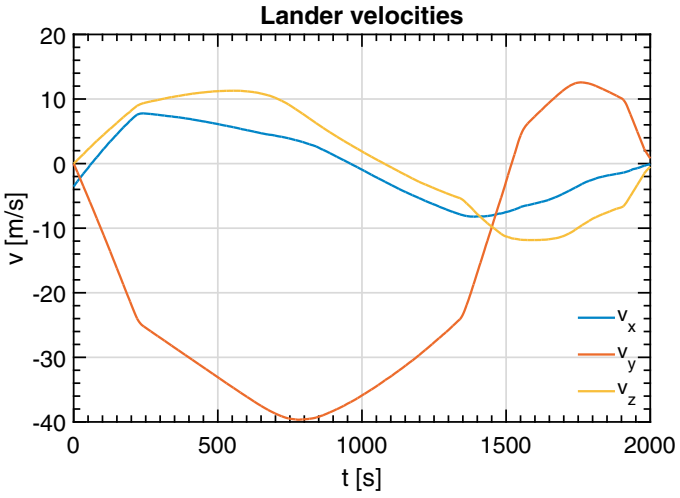

Fig. 4. Lander velocities.

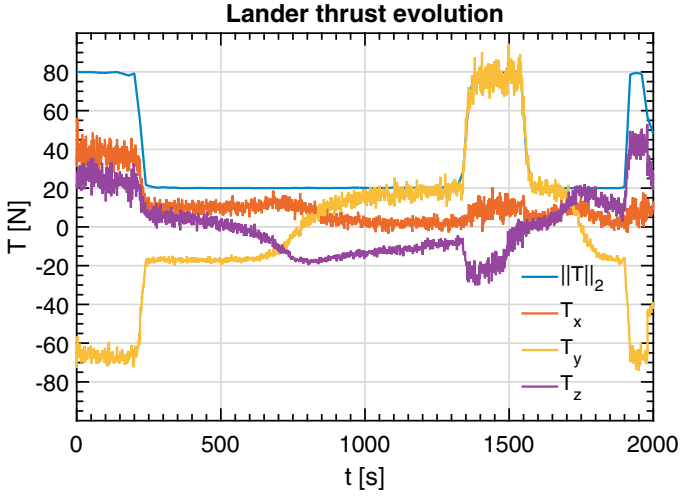

Fig. 6. Computed thrust norm (blue) and applied thrust components.